

Retrieval Robust to Object Motion Blur

Rong Zou¹, Marc Pollefeys^{1,2}, and Denys Rozumnyi^{1,3}

¹ ETH Zürich

² Microsoft

³ Czech Technical University in Prague

Abstract. Moving objects are frequently seen in daily life and usually appear blurred in images due to their motion. While general object retrieval is a widely explored area in computer vision, it primarily focuses on sharp and static objects, and retrieval of motion-blurred objects in large image collections remains unexplored. We propose a method for object retrieval in images that are affected by motion blur. The proposed method learns a robust representation capable of matching blurred objects to their deblurred versions and vice versa. To evaluate our approach, we present the first large-scale datasets for blurred object retrieval, featuring images with objects exhibiting varying degrees of blur in various poses and scales. We conducted extensive experiments, showing that our method outperforms state-of-the-art retrieval methods on the new blur-retrieval datasets, which validates the effectiveness of the proposed approach.

Keywords: object retrieval, object motion blur, datasets

1 Introduction

The task of image retrieval has long been a focal point in computer vision research, aiming to efficiently identify images within a large-scale database that share similarities with a given query image. In the realm of image retrieval, methods are often categorized into category-level and instance-level retrieval. We focus on the latter, where the objective is to identify images of a specific object featured in a query within a vast, unordered collection of database images. In this task, image representations play an important role since they capture the essence of the objects in images and enable the measurement of their similarities. Representing images based on hand-crafted features has been extensively studied [3, 21]. Owing to the development in deep learning, recent strides have been made in adopting learning-based approaches to encode image content [2, 4, 20, 24, 29, 40, 42, 46, 47]. However, the current literature focuses exclusively on image representations for sharp objects, assuming that the objects are stationary and clearly visible in images. By only considering sharp and static objects, the existing retrieval methods fall short in addressing the dynamic nature of real-world scenarios, where objects are in movement, resulting in images blurred by object motion — a phenomenon prevalent in environments with fast-moving objects [31, 33], low camera frame rates, and extended exposure times.

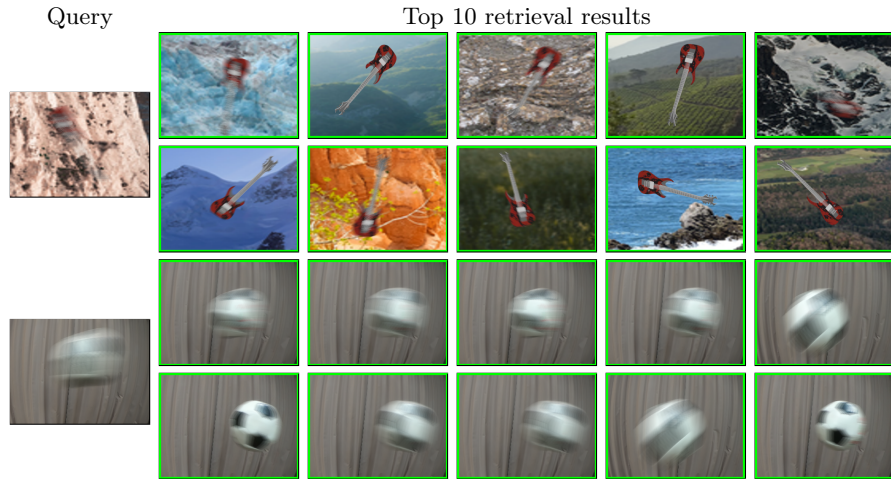


Fig. 1: Retrieval robust to object motion blur. We present the first approach designed for retrieval in the presence of object motion blur. Our method is capable of capturing blur-invariant features and generates blur-robust representations. We show retrieval results on the newly created datasets for the task of blur-robust retrieval: synthetic (top) and real (bottom). All retrieved images are positive matches with the query and are marked with green boxes.

To bridge this gap, we introduce a novel task in image retrieval: *retrieval with object motion blur*. The challenge of this task lies in finding image representations that are robust to object motion blur, in addition to other variations such as background and changes in viewpoint. We also propose the first approach targeting this task that produces representations invariant to motion blur. In response to the unique challenge posed by object motion, we propose loss functions designed to enhance the model’s comprehension of blur, thereby ensuring robust retrieval performance even under conditions of extreme blurring, as seen in Fig. 1.

Recognizing the absence of datasets accommodating images with motion-blurred objects in existing retrieval benchmarks, we introduce the first benchmark datasets for this task, which include a synthetic dataset for training and a real-world dataset created specifically for evaluation. By re-training and evaluating state-of-the-art instance retrieval methods on this comprehensive benchmark, we reveal their shortcomings in handling motion-blurred scenarios.

This work marks a key step in advancing practical methods for object retrieval in the challenging presence of motion blur. It has potential applications in fields such as endangered wildlife monitoring, sports analysis, and security surveillance.

To summarize, our main contributions are as follows:

- (1) We present the first method specifically designed for the novel retrieval task involving object motion blur. The method is trained with loss functions tailored to improve its understanding of motion blur.

- (2) We introduce a new benchmark featuring synthetic and real-world datasets specifically constructed for this task. The datasets are carefully processed and are directly applicable for future research in blur retrieval.
- (3) We conducted extensive experiments and detailed analyses to validate the effectiveness of our approach. Our method outperforms state-of-the-art retrieval methods and demonstrates superior robustness to motion blur.

2 Related work

Standard retrieval. In the domain of standard image retrieval, local feature-based methods have evolved from traditional hand-crafted techniques, such as SIFT [21] and SURF [3], to contemporary deep learning-based approaches like DELF [24] and HOW [40]. Considering that in our task, local information of objects can be corrupted due to motion blur and thus local descriptors may not be robust, we adopt a global approach. Classical methods obtain global features mainly by aggregating hand-crafted local features with aggregation techniques such as BoW [37], Fisher vectors [26], VLAD [15], AMSK [39], *etc.* Modern deep learning-based approaches generate global descriptors by performing various pooling operations on the feature maps encoded by convolutional neural networks (CNNs), such as sum pooling [1, 41], weighted sum pooling [16], max pooling, regional max pooling [42], and generalized mean-pooling (GeM) [29], which has been widely adopted in the recent literature [4, 20, 47]. Our method leverages insights from recent advancements in global feature methods, adopting GeM pooling [29] for feature extraction and incorporating contrastive loss [6] and ArcFace loss [9] during training.

Among the single-pass global feature-based methods, DELG global branch [4], DOLG [47] and Token [46] are the state-of-the-art standard retrieval methods. However, these methods face challenges when handling images involving motion blur, leading to a degradation in performance. Our work stands out in addressing the significant gap in the literature, as existing retrieval methods overlook the impact of motion blur. To bridge this research gap, we propose novel loss functions aimed at enhancing the model’s comprehension of motion blur, thereby contributing to the advancement of image retrieval in the presence of motion blur.

Blur handling. Handling blur in images is an important topic in computer vision. [43] investigates the effect of different types of blur (de-focus, uniform subject motion, camera shake) on the performance of CNNs for image classification and semantic segmentation. [36] studied online object detection under the influence of camera ego-motion-induced blur. Image and video deblurring are long-standing tasks in computer vision, which have been addressed by a variety of methods [10, 19, 44, 49, 50]. Joint deblurring and trajectory estimation for motion-blurred objects have also been extensively explored, with notable contributions from methods like [18, 30, 32, 33], some extending their scope to 3D reconstruction [34, 35]. It is worth noting that these existing works predominantly focus on other types of blur or address distinct tasks, emphasizing the

need for specialized efforts in the context of our targeted task of retrieval in the presence of object motion blur.

Datasets. Several datasets have been proposed that contain generic corruptions including blur, such as ImaneNet-C [13] and Coco-C [22], but they do not focus purely on blurry images, and the type of blur considered in those datasets is not induced by object motion. Many datasets contain blurry-sharp image pairs, such as RealBlur [14] and GoPro [23], but they are created for deblurring tasks and not for retrieval, and the blur in images is mainly caused by camera motion or camera shake, not by object motion. A large variety of standard retrieval datasets have been proposed, including Revisited Oxford5k and Paris6k [27], Google Landmarks V2 [45, 48], SfM120K [28], etc. However, none of them incorporate motion-blurred images. To the best of our knowledge, there is currently no existing dataset tailored for the blur retrieval task. In view of this, we created a synthetic and a real-world dataset specifically designed for the novel task of blur retrieval.

3 Method

We perform retrieval via nearest neighbor search in a representation space. Therefore, we require a representation model that is robust to object motion blur. We train a deep learning-based model that maps images to a vector space. The network is trained on our proposed synthetic dataset using multiple losses, including those tailored to object motion blur. As we show, the method generalizes well to real data despite being trained on synthetic data.

The network takes an RGB image $\mathbf{I} \in \mathbb{R}^{3 \times H \times W}$ containing a sharp or blurred object as input and generates a descriptor $\mathbf{D} \in \mathbb{R}^d$ robust to object motion blur through the *Blur Robust Image Descriptor Generator* module (BRIDGE, Sec. 3.1). For training only, contrastive samples are selected by the *Blur Level-based Image Sample Selection* mechanism (BLISS, Sec. 3.2) based on the query blur level b_q and the contrast blur level range r . The selected image samples are sent into the BRIDGE module to extract descriptors for contrastive learning. The architecture of the proposed blur retrieval method is shown in Fig. 2.

3.1 BRIDGE module

The BRIDGE module encodes an image to a descriptor that is robust to object motion blur. The input image is encoded by a ResNet-50 backbone [12] to produce a feature map $\mathbf{\Omega} \in \mathbb{R}^{C \times U \times V}$. Then, we use GeM pooling [29] to process the feature map into a feature vector $\mathbf{f} \in \mathbb{R}^C$, expressed as

$$\mathbf{f} = \left[\left(\frac{1}{|\mathbf{\Omega}|} \sum_{(u,v) \in \mathbf{\Omega}} x_{(c,u,v)}^p \right)^{\frac{1}{p}} \right]_{c=1, \dots, C}, \quad (1)$$

where $p > 0$ is a parameter, and setting it to values larger than 1 forces the pooled vector to focus on the salient areas. This feature vector then undergoes

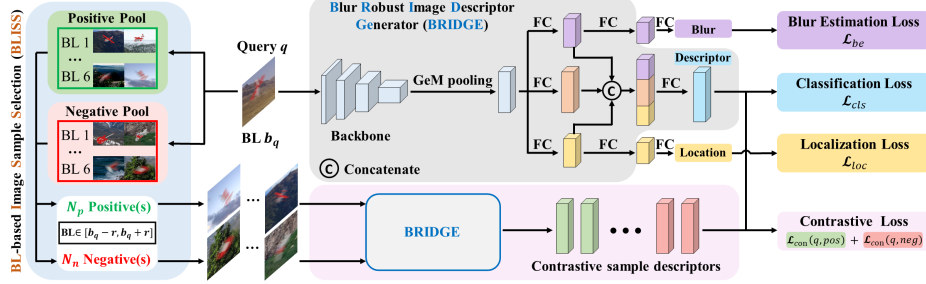


Fig. 2: Overview of the proposed method for blur-robust retrieval. Our model takes a query image as input. Then, it generates a descriptor robust to object motion blur through the *Blur Robust Image Descriptor Generator* (BRIDGE) module that encodes the input image using a CNN backbone followed by generalized mean-pooling (GeM) [29], extracting a feature vector. This vector is subsequently fed into three heads: the blur estimation head, classification head, and localization head. Each head processes the feature vector to extract relevant information for identifying motion-blurred objects. The resulting three processed feature vectors are concatenated and passed through the final fully connected (FC) layer to produce the blur-robust descriptor. During training, the *Blur Level-based Image Sample Selection* (BLISS) mechanism is employed to select contrastive samples based on the query blur level (BL, Eq. (6)) b_q and a specified blur level range r . Then, these selected image samples are input into the BRIDGE module to extract descriptors for subsequent contrastive learning.

multi-head processing to generate a motion blur-robust descriptor. Specifically, in the blur estimation head, we obtain blur estimation features $\mathbf{f}_{be} \in \mathbb{R}^{C_b}$ by a fully connected (FC) layer. The same dimension reduction is performed in the localization head, which generates features for location prediction $\mathbf{f}_{loc} \in \mathbb{R}^{C_l}$. The features generated from the two heads are then concatenated with the whitened [11] features $\mathbf{f}_{cls} \in \mathbb{R}^{C_c}$ from the classification head. We further reduce the dimension of the concatenated features to obtain the final blur-robust descriptor of the image. This can be expressed as:

$$\mathbf{D} = \mathbf{W} \cdot \text{Concat}(\mathbf{W}_{be}\mathbf{f}, \mathbf{W}_{loc}\mathbf{f}, \mathbf{W}_{cls}\mathbf{f}), \quad (2)$$

where $\mathbf{W}_{be} \in \mathbb{R}^{C_b \times C}$, $\mathbf{W}_{loc} \in \mathbb{R}^{C_l \times C}$ and $\mathbf{W}_{cls} \in \mathbb{R}^{C_c \times C}$ represent the weights of the FC layers in the blur estimation, localization, and classification heads, respectively, and $\mathbf{W} \in \mathbb{R}^{d \times (C_b + C_l + C_c)}$ is the weight of the final dimension-reduction layer.

3.2 BLISS mechanism

While the specific representation of the degree of motion blur for objects in images is yet to be formally defined, it is intuitively perceived as a continuous value. The level of detail exhibited by objects varies with the degree of blur: sharper objects show clear structures, textures, and poses, while more blurred objects primarily reveal color characteristics (see Fig. 3). This continuous nature

of blur allows us to indirectly control the distance between samples with significantly different blur conditions during learning image representations. In this context, we manage the distance between samples that exhibit visual features and patterns of the same level of detail due to similar degrees of blur, thus indirectly influencing the distance between samples with significantly different levels of blur. Additionally, we can directly control the distance between samples with large differences in blur conditions by imposing constraints directly between such samples in the descriptor space. There are therefore two key research questions: What is the optimal value for the range of differences in the blur levels of image pairs used in contrastive learning? How does adjusting the range of differences in blur levels affect the model’s performance? To answer these questions and identify the optimal blur level range for contrastive learning, we introduce the BLISS mechanism. This mechanism selects contrastive samples based on the blur level in the query image for contrastive learning.

Blur severity definition. Our definition of blur severity is inspired by the image generation process. The formation of an image \mathbf{I} containing a motion-blurred object in front of a background can be expressed [31] as

$$\mathbf{I} = \mathbf{P} * \mathbf{O} + (1 - \mathbf{P} * \mathbf{M})\mathbf{B} \quad (3)$$

where the first term denotes the convolution ($*$) of a point spread function \mathbf{P} corresponding to a motion trajectory and the object’s sharp appearance \mathbf{O} , and the second term depicts the contribution of the background \mathbf{B} , in which \mathbf{M} is the binary mask of \mathbf{O} . Let

$$\alpha = \mathbf{P} * \mathbf{M}, \quad (4)$$

$\alpha \in \mathbb{R}^{H \times W}$, $\alpha(i, j) \in [0, 1], \forall (i, j) \in \mathbf{I}$. Considering only objects with opaque materials, α represents the visibility of the object. In other words, it can characterize the amount of blur. Generally, the sharper the object in the image, the larger the α values are. However, at the edge pixels, the object blends with the background, and the alpha values of these edge pixels gradually fade to 0. Combining the alpha mask Eq. (4) and considering edge effects, we define the blur severity of an image with a motion-blurred object as:

$$BS = 1 - \frac{\sum_{i=1}^H \sum_{j=1}^W \beta(i, j) \cdot \alpha(i, j)}{\sum_{i=1}^H \sum_{j=1}^W \beta(i, j)}, \quad (5)$$

where β is a thresholded (by 0) and eroded (by 3 pixels) binary mask of α . Erosion effectively removes the adverse contribution of the edge pixels to the blur severity measure. As a result, $BS \in (0, 1)$, and the larger the value, the more severe the motion blur in the image.

Blur level-based sample selection. Since blur severity is a continuous quantity, finding images within a certain blur severity range for each query image is expensive. We thus use a discretized version of blur severity – *Blur Level* (BL):

$$BL = \lceil 10BS \rceil, \quad (6)$$

where $\lceil \cdot \rceil$ denotes ceiling operation. Each image is assigned to a BL according to its BS . During training, we select contrastive samples based on the query blur level b_q and the specified contrastive BL range r . The selected N_p positive and N_n negative samples therefore have blur levels within the range of $b_q - r$ to $b_q + r$.

3.3 Training objectives

Blur estimation loss. Blur severity contains information about the visibility of the blurred object in an image (Sec. 3.2). From another perspective, it can be viewed as a signal-to-noise ratio that indicates the object-to-background ratio. In view of this, we define blur estimation loss as

$$\mathcal{L}_{be} = |p - (1 - BS)|, \quad (7)$$

where $p \in \mathbb{R}$ is the blur value predicted by the blur estimation head. By constraining the estimate of the continuous BS (Eq. (5)) instead of the discrete BL (Eq. (6)), we implicitly force the network to estimate an accurate object-to-background ratio at each pixel point, which helps to extract object information in the blurred region.

Localization loss. This loss is defined as

$$\mathcal{L}_{loc} = |x - \hat{x}| + |y - \hat{y}| + |h - \hat{h}| + |w - \hat{w}|, \quad (8)$$

where (x, y, w, h) and $(\hat{x}, \hat{y}, \hat{w}, \hat{h})$ represent the normalized ground truth bounding box and the estimated one from the localization head, respectively. Localization loss forces the network to distinguish between motion-blurred objects and backgrounds under various blurring conditions. It takes advantage of the pixel-level precise labeling of synthetic data to enhance the network’s understanding of blur.

Classification loss. Following DELG [4], we apply ArcFace margin loss [9] to the descriptor \mathbf{D} , expressed as

$$\mathcal{L}_{cls} = -\log \left(\frac{\exp(\gamma \times AF(\hat{\mathbf{w}}_t^T \hat{\mathbf{D}}, 1))}{\sum_n \exp(\gamma \times AF(\hat{\mathbf{w}}_n^T \hat{\mathbf{D}}, y_n))} \right), \quad (9)$$

where γ is a scale factor, $\hat{\mathbf{w}}_i$ refers to the i -th row of the L_2 normalized N -class classifier $\hat{\mathbf{W}} \in \mathbb{R}^{d \times N}$, $\hat{\mathbf{D}}$ denotes the L_2 normalized \mathbf{D} . y is the one-hot label, and t represents the ground truth class index ($y_t = 1$). AF is the ArcFace-adjusted cosine similarity and it can be expressed as

$$AF(s, g) = \begin{cases} \cos(\arccos(s) + m), & \text{if } g = 1 \\ s, & \text{if } g = 0 \end{cases}, \quad (10)$$

where s is the cosine similarity, m is the ArcFace margin, and $g \in \{0, 1\}$. $g = 1$ indicates the ground truth class.

Dataset	#Images Total	#Images by BL (Syn.) or BL ^r (Real)					
		1	2	3	4	5	6
Syn. Q	20995	4288	3932	4078	4089	2930	1678
Syn. DB	91621	18871	17508	17888	18029	12546	6779
Real Q	2753	612	620	561	396	315	249
Real DB	10340	1923	1803	2080	1745	1375	1414

Table 1: Distribution of images in our synthetic and real datasets, sorted by blur levels. ‘Q’ stands for ‘query’ and ‘DB’ for database.

Contrastive loss. We employ contrastive learning [6] to construct a descriptor space, where the distance between similar samples is minimized, and between dissimilar samples maximized. The contrastive loss is applied to $(query, positive)$ and $(query, negative)$ descriptor pairs:

$$\mathcal{L}_{con}(i, j) = \begin{cases} 0.5 \cdot D_{i,j}^2, & \text{if } y(i, j) = 1 \\ 0.5(\max\{0, \tau - D_{i,j}\})^2, & \text{if } y(i, j) = 0 \end{cases}, \quad (11)$$

where $D_{i,j} = \|\hat{\mathbf{D}}(i) - \hat{\mathbf{D}}(j)\|$ and $\hat{\mathbf{D}}(i)$ is the L_2 normalized descriptor of image i . τ is a margin parameter, and $y(i, j)$ is binary indicating whether the pair matches ($= 1$).

Joint loss. The joint loss is a weighted sum of all previously defined loss functions:

$$\mathcal{L}_{joint} = \mathcal{L}_{con} + \alpha_{cls}\mathcal{L}_{cls} + \alpha_{be}\mathcal{L}_{be} + \alpha_{loc}\mathcal{L}_{loc}. \quad (12)$$

4 Dataset

We create novel synthetic and real datasets for training and evaluation of retrieval methods for motion-blurred objects. The synthetic dataset is used for both training and evaluation. We also generate a large-scale synthetic distractor set to evaluate the methods in a more challenging condition. Furthermore, we recorded a novel real-world dataset to validate the effectiveness of our method in real scenarios. All datasets are meticulously processed specifically for the task of blurry retrieval, laying a crucial foundation for future research. The datasets will be publicly released. Statistics of both datasets are shown in Table 1.

4.1 Synthetic dataset

The images in this dataset contain 3D objects moving along different 6D trajectories, at different amounts of motion blur, and in front of different backgrounds. Thus, this dataset poses many challenges to retrieval methods.

Backgrounds. Background images are sampled from the LHQ dataset [38], cropped to a resolution of 240×320 .

Objects. We select 39 categories with the largest number of textured objects from the ShapeNet dataset [5] and randomly sample 30 objects for each class.

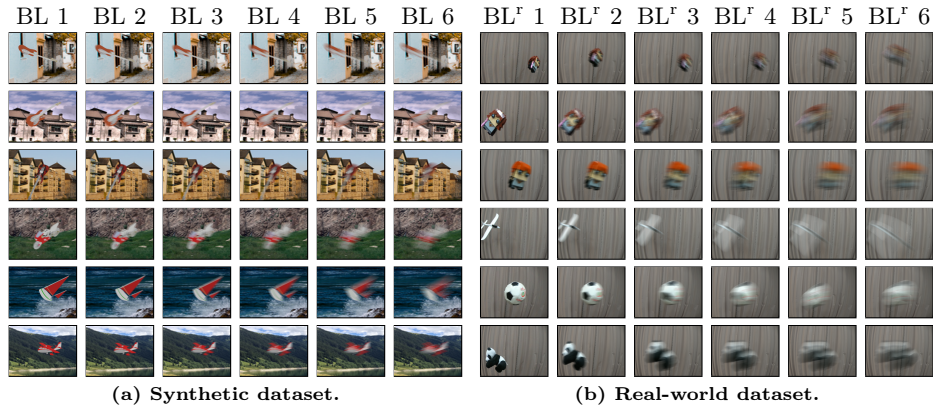


Fig. 3: The introduced synthetic (a) and real-world (b) datasets. Rows 1-2: different trajectories of the same object. Rows 2-3: two different objects from the same category with similar shapes. Rows 4-6: objects from different categories but share similar textures. Columns correspond to different blur levels, from 1 to 6, and they are different for synthetic (BL) and real-world (BL^r) datasets.

Trajectories. For each object, we randomly generate 120 6D trajectories with linear 3D translation and linear 3D rotation. Each trajectory is split into 23 sub-trajectories. Then, we select up to 10 consecutive sub-trajectories to generate images featuring objects with diverse levels of motion blur.

Rendering. We render blurry images with Blender Cycles [7] by capturing moving objects during the camera exposure time. Additionally, we render one sharp image per trajectory, placed at the central position along the trajectory.

Filtering. We filter out renderings if the number of pixels occupied by the object is less than 1.5% or if the intersection-over-union between silhouette renderings at trajectory endpoints is below 20%. The former condition suggests that the object is too small, while the latter indicates that the appearance of the object changes too much.

Ground truth. For each of the generated images, we estimate the bounding box coordinates by detecting the non-zero pixels in the alpha channel. We calculate the blur level for each image based on Eq. (6).

Retrieval dataset. In total, we rendered 1.5 million images for 1138 different instances (examples in Fig. 3a).

Distractor set. Additionally, we generate a challenging distractor set with 1.2 million images. We use the same object categories as in the synthetic training dataset to increase the difficulty of the distractors in terms of intra-class similarity. We randomly select 40 objects for each category after excluding the 30 previously chosen objects in the training dataset. We generate 70 trajectories for each object. For each trajectory, we render one sharp image and 10 blurry images with varying amounts of blur. Backgrounds are also chosen from a different subset of [38].

Method	mAP by query BL (synthetic)						mAP by query BL (synthetic + 1M)							
	All	1	2	3	4	5	6	All	1	2	3	4	5	6
DELG [4]	81.65	83.55	84.96	84.89	82.69	77.35	66.20	68.19	73.64	75.40	73.34	68.05	58.28	42.46
DOLG [47]	83.03	85.10	86.26	85.93	84.04	78.78	68.07	69.97	75.75	77.47	75.01	70.10	60.01	42.49
Token [46]	84.84	86.53	87.99	87.50	85.81	80.70	71.57	70.65	75.32	77.66	75.51	70.24	61.19	48.05
Ours-sharp	27.57	43.06	38.53	29.74	19.40	10.87	6.14	32.64	71.93	43.88	27.18	15.41	7.94	4.27
Ours	91.78	93.05	93.48	93.14	92.25	90.20	82.86	84.09	88.74	89.56	87.68	84.41	76.89	62.42

Table 2: Retrieval results on the synthetic dataset with (+1M) and without distractors. Ours-sharp is our model trained with only sharp images. 'All' denotes the overall performance for queries of all blur levels. All methods are re-implemented and re-trained on our synthetic training set. The database contains images of all blur levels. The highest scores are marked in bold.

4.2 Real-world dataset

We record videos with a GoPro 7 Hero camera at 240 fps with full exposure. We use 35 different objects and move each object 3 to 5 times along different trajectories in front of the camera. In total, we recorded 139 videos. Different amounts of blur are generated by averaging consecutive frames, ranging from just one up to 200 averaged frames.

Computing blur level based on Eq. (6) is not feasible for the real-world dataset. Therefore, we manually annotate the data, assigning each image to one of 6 blur levels, and we use the ratio of the trajectory length to the average object size as a reference. Since the blur level for real data is different from the blur level from Eq. (6), we denote it as BL^r .

The real-world dataset contains 13,093 images, with an average of 374 images for each object (examples in Fig. 3b). Compared to the synthetic dataset, the object scale change is more drastic in different trajectories, *e.g.* rows 1 & 2. The trajectories are no longer linear in their 3D translation and 3D rotation as in the synthetic dataset, but more complex curved trajectories with acceleration and other forces, which poses an additional challenge for methods trained on our synthetic dataset.

5 Experiments

Setup. For each category of objects in the synthetic dataset, we randomly take 70% (rounded down, same for validation) for training (792 objects), 15% for validation (153 objects), and 15% for testing (193 objects). For the training objects, we take one image for each trajectory while ensuring a balanced distribution of images across different blur levels. In total, there are 95k images in the training set. For each of the test objects, we sample 20 trajectories to form a query set, and the rest is used for the database. The database images are sampled from all blur levels unless specified otherwise (for per blur level database experiment). We additionally show performance on a subset of queries for a given blur level. In all experiments (except Ours-sharp), only one model is trained for all blur levels, and the evaluation is performed for varying blur levels.

Method	mAP	mAP by Query BL ^r					
	All	1	2	3	4	5	6
DELG [4]	54.82	49.13	63.43	57.25	55.01	53.77	42.92
DOLG [47]	54.64	43.93	60.59	58.36	59.06	58.58	45.78
Token [46]	43.33	38.71	47.08	50.79	46.44	42.71	24.43
Ours-sharp	40.24	49.55	45.02	41.33	33.23	29.40	27.91
Ours	62.88	57.50	70.38	66.77	63.18	64.48	46.14

Table 3: Retrieval results on the real-world dataset (trained on synthetic). Our method outperforms other methods.

Implementation details. The proposed method is implemented in PyTorch [25]. We use ResNet-50 [12] up to the last downsampling block as the backbone, deactivate the normalization layers, and initialize the model with ImageNet [8] pre-trained weights. ADAM [17] optimizer is employed to minimize the joint loss with a fixed learning rate 10^{-4} , batch size 32, and 30 epochs. We initialize the power parameter to 3 for GeM pooling [29]. The contrastive margin τ is set to 0.7. Following [29], we set the number of contrastive samples as $N_p = 1$, $N_n = 5$. The contrastive blur range is experimentally set to 5. For the classification loss, we empirically set the margin m to 0.15 and the scale γ to 30. Loss weights are chosen such that the values of different losses are approximately within the same magnitude, *i.e.* $\alpha_{cls} = 0.1$, $\alpha_{be} = 1.0$, $\alpha_{loc} = 10$. The descriptor dimension d is set to 128.

Evaluation protocols. We report mean average precision (mAP@all) as commonly used in retrieval. In case 1M additional distractors are used, we report mAP@100 (top 100).

Compared methods. Since retrieval in the presence of object motion blur has not been addressed before, there are no methods specifically designed for this task. Therefore, we compare to state-of-the-art standard retrieval methods, namely DELG-global [4] (referred to as DELG), DOLG [47], and Token [46]. All these methods are re-implemented as in the original papers, except for changing the size of the output descriptors to 128 for fair comparison. We re-train the compared methods using the same ArcFace parameters and on the same synthetic data as our method.

5.1 Results

All blur levels in the database. The proposed method outperforms all state-of-the-art retrieval methods for all settings, as shown in Table 2 on synthetic data and in Table 3 on real data. Our model exhibits substantial superiority over the state-of-the-art retrieval approaches without adding complex computation modules, which demonstrates the effectiveness of the proposed loss functions. Results on the real-world dataset show that our method generalizes well to real data even when trained only on synthetic. Additionally, we train a version of our method where only sharp images are used (Ours-sharp). When evaluating with mAP@all (no distractors), it fails completely, especially for higher blur

BL D \ Q	DELG [4] (range: 57.79; std: 16.75)							DOLG [47] (range: 56.81; std: 16.93)						
	All	1	2	3	4	5	6	All	1	2	3	4	5	6
1	75.99	86.73	84.17	80.26	72.48	63.12	50.08	77.78	87.01	85.70	81.85	75.11	66.20	52.39
2	77.35	82.74	86.22	82.87	76.68	66.46	50.00	78.44	84.18	87.00	83.43	77.91	67.88	51.31
3	77.19	79.62	83.43	82.94	78.46	69.43	52.86	78.49	81.84	84.74	83.85	79.69	70.58	53.12
4	74.96	74.26	78.91	79.85	78.05	70.89	55.12	76.40	77.27	80.55	80.80	79.10	71.73	55.28
5	62.71	57.86	61.72	64.37	65.36	68.96	56.05	64.19	61.31	63.68	65.38	66.05	69.68	55.75
6	34.89	29.56	28.94	31.75	34.06	45.37	53.86	35.51	31.24	30.20	32.29	34.18	45.00	53.41

BL D \ Q	Token [46] (range: 55.72; std: 16.11)							Ours (range: 53.68 ; std: 15.65)						
	All	1	2	3	4	5	6	All	1	2	3	4	5	6
1	79.65	88.22	87.34	83.50	76.87	68.51	56.63	88.57	95.09	94.24	91.54	87.19	80.91	68.15
2	79.97	84.78	88.48	84.77	78.99	70.01	55.82	88.75	93.07	94.65	92.18	88.77	82.03	67.18
3	79.50	81.79	85.46	84.75	80.21	72.09	58.18	88.76	91.70	93.18	92.32	89.83	83.41	68.94
4	76.82	76.56	80.42	81.24	79.31	72.61	59.61	87.16	88.12	90.11	90.09	89.31	84.37	70.35
5	65.39	61.85	64.49	66.31	67.14	70.96	60.36	76.28	73.87	74.90	76.04	77.39	83.06	71.67
6	37.98	33.23	32.76	34.61	36.50	47.56	57.43	47.31	43.43	41.41	42.89	44.55	58.13	69.59

Table 4: Retrieval results by query (Q) and database (D) blur level (BL) on our synthetic dataset (with 1M distractors). 'All' denotes the overall performance for queries of all blur levels. The standard deviation and range of mAP values is shown next to each method. The best scores under the same settings are marked in bold.

levels. When evaluating with mAP@100 (with distractors), it achieves reasonable results on query BL 1 and 2, but still worse than all other methods. This demonstrates the need for specifically designed methods and training datasets with highly motion-blurred objects.

Per blur level database. In this setup, we utilize datasets specific to each blur level, considering them as individual subsets of images with the designated blur level, to form the database. We then assess the retrieval performance by using query images with distinct blur levels, resulting in a comprehensive evaluation comprising 36 results (6 database BLs by 6 query BLs) for each method. We also compute the standard deviation (std) and range of mAP for different settings per method, reflecting the robustness of each method to different levels of motion blur. The proposed method outperforms all other state-of-the-art methods for all settings and also achieves the smallest standard deviation and range, showing the highest robustness to motion blur (Table 4).

Qualitative results on our proposed synthetic (Fig. 4a) and real-world (Fig. ??) datasets. The proposed method is compared to the best-performing (per query) state-of-the-art retrieval methods, which yield a substantial number of false positives that have similar textures to the motion-blurred object in the query image. In contrast, our method is able to correctly retrieve positive images despite extreme motion blur in the query and the presence of many challenging distractors. Note that the positive images retrieved by standard retrieval methods have only blur levels similar to the query, whereas our method retrieves correct images with a large variety in blur levels (from 1-6 for synthetic and 2-6 for real). This indicates that our method is able to learn invariant representations of the same object under different blur levels.

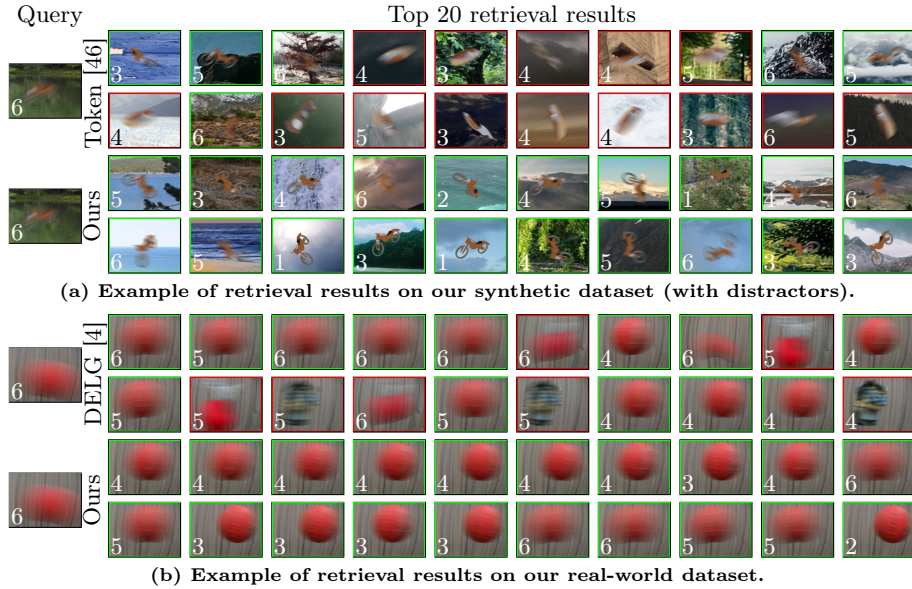


Fig. 4: Comparison of retrieval results. We compare to the best-performing state-of-the-art method for the corresponding query. The retrieved images are sorted from left to right, top to bottom, with the ranking from the 1st to the 20th. The blur level of each image is shown in bottom left corner. Correct results are indicated with green boxes, while incorrect ones are marked with red boxes.

5.2 Ablation study

Loss components. Table 5 shows an ablation study of different loss functions. The results show that all loss functions improve the performance of the model. We highlight that the performance of our model outperforms the state-of-the-art across all query blur levels (Table 2), even when utilizing only three out of the four loss terms *at any combination*. For instance, when using \mathcal{L}_{con} , \mathcal{L}_{cls} and \mathcal{L}_{be} , the mAP of our method exceeds mAP of Token [46] by 2.50 in BL1 and 1.91 on BL6, with an overall improvement of 2.33.

Contrastive range. In this analysis, we specifically address the research questions posed in Sec. 3.2. The results of using different blur level ranges for contrastive learning are shown in Table 6. As shown, a broader range of contrastive blur levels enhances the model’s performance, with the highest mAP achieved at the maximum range of 5.

Design of blur estimation loss. We validate the effectiveness of our design of blur estimation loss \mathcal{L}_{be} (Eq. (7)) in Table 6. We compare with the case where edge effects are ignored in the loss function. This corresponds to directly predicting the average of the entire alpha mask (Eq. (4)) inside the object boundary. The results show that our design of \mathcal{L}_{be} , which effectively mitigates the detrimental impact of edge blur, improves the model’s retrieval performance.

\mathcal{L}_{con}	\mathcal{L}_{cls}	\mathcal{L}_{be}	\mathcal{L}_{loc}	mAP All	mAP by Query BL					
					1	2	3	4	5	6
✓	✗	✗	✗	78.13	80.51	81.70	81.16	79.20	73.93	61.24
✓	✗	✓	✗	81.66	83.49	85.01	84.43	82.69	77.64	67.08
✓	✗	✗	✓	85.94	87.54	88.25	87.83	86.52	83.08	75.58
✓	✗	✓	✓	87.48	88.69	89.89	89.40	88.24	84.97	76.74
✗	✓	✗	✗	78.73	81.53	82.97	82.83	79.86	72.93	59.00
✗	✓	✓	✗	83.67	85.19	87.56	87.40	85.10	79.22	65.93
✗	✓	✗	✓	88.74	89.89	90.91	90.88	89.75	86.07	77.67
✗	✓	✓	✓	91.23	92.02	93.16	93.09	91.97	89.00	82.27
✓	✓	✗	✗	85.06	87.42	88.29	87.66	85.85	81.20	69.96
✓	✓	✓	✗	87.17	89.03	90.03	89.55	88.07	83.91	73.48
✓	✓	✗	✓	90.39	91.85	92.45	92.14	91.20	88.20	79.36
✓	✓	✓	✓	91.78	93.05	93.48	93.14	92.25	90.20	82.86

Table 5: Ablation study of different loss components on the synthetic dataset. The database contains images of all blur levels.

Cont. BL Range	mAP All	mAP by query BL					
		1	2	3	4	5	6
S	82.26	87.37	88.46	86.29	82.61	74.13	58.26
M	83.33	87.97	89.12	86.93	83.87	76.04	60.61
L	84.09	88.74	89.56	87.68	84.41	76.89	62.42
L (alpha)	82.83	87.62	88.68	86.43	82.96	75.68	60.27

Table 6: Ablation study of different blur level ranges in contrastive learning and design of blur estimation loss. **Small**: range=1. **Medium**: range=3. **Large**: range=5. Alpha corresponds to the alternative design choice for blur estimation loss. The database contains images of all blur levels.

6 Conclusion

In this paper, we introduce an innovative task: image retrieval in the presence of object motion blur. To tackle this challenge, we propose a global retrieval approach that integrates specialized loss functions tailored to better comprehend motion blur. Our method stands as the first specifically designed solution for this new task. Moreover, we introduce the first benchmark datasets for blur retrieval, comprising both synthetic and real-world data. These datasets are meticulously processed and annotated to ensure their immediate applicability for future research in this emerging area. Through extensive experiments conducted on these benchmark datasets, we demonstrate the limitations of state-of-the-art retrieval methods in handling motion-blurred images and showcase the superior performance and robustness of our proposed approach in accurately retrieving images even in challenging motion-blurred scenarios.

Acknowledgement. Rong Zou would like to thank Giorgos Tolas for the highly valuable discussions with him and the support he provided for this work.

Retrieval Robust to Object Motion Blur (Supplementary Material)

Rong Zou¹, Marc Pollefeys^{1,2}, and Denys Rozumnyi^{1,3}

¹ ETH Zürich

² Microsoft

³ Czech Technical University in Prague

1 Details of distractor set

Examples from our distractor set are presented in Fig. 1. For every query example, we display 8 negative images from the distractor set. In addition, we include 2 positive images from the database: one blurred and another in a sharp state. These examples vividly illustrate the obfuscation caused by object motion blur, highlight the challenging nature of the distractors, and underscore the inherent difficulty of the blur retrieval task introduced in this study.

2 More quantitative results

2.1 Per BL database results (without distractors)

We show detailed per blur level database retrieval results of our method and state-of-the-art approaches on our synthetic dataset (without distractors) in Table 1. For a clearer representation of the trend in retrieval performance with varying database and query blur levels, as well as a more intuitive comparison among different methods, we cluster the retrieval results in Table 1 according to the database blur level. The visualization of these results for each specific database blur level is presented in Fig. 2, where we additionally provide results for Ours-sharp (the version of our model trained with only sharp images).

Figure 2 clearly shows that our method outperforms others across all settings. Notably, at lower database blur levels, the performance gap between our method and others becomes more noticeable as the query blur level increases, while at higher database blur levels, this gap remains pronounced for both low and high query blur levels. This highlights the significant advantage of our method in handling images affected by severe object motion blur. Furthermore, it can be observed that our method exhibits overall minimal performance fluctuations with changing query blur levels across various database blur levels, as evident from the range and standard deviation values in Table 1, indicating that our method has the highest robustness for retrieving images in the presence of object motion blur compared to state-of-the-art retrieval methods.

Regarding the model trained solely with sharp images, it produces reasonable results only when both the database and query blur levels are low. Its performance rapidly declines as the database blur level increases, which emphasizes

the significance of training with images containing motion-blurred objects for effective retrieval in the context of object motion blur.

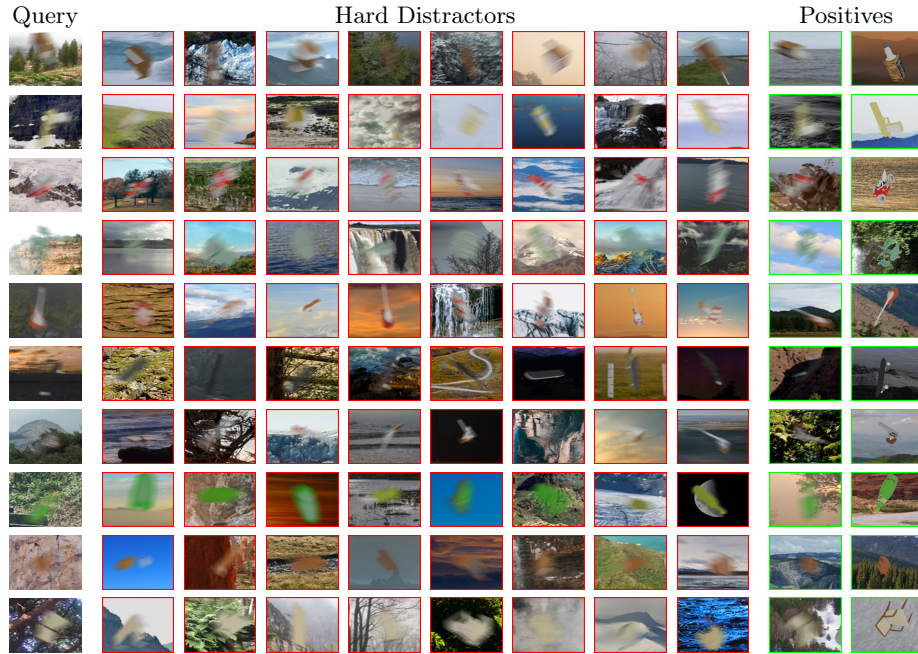


Fig. 1: Examples of hard distractors in our distractor set. Each row displays a query image on the left, 8 hard distractors in the middle (marked with red boxes), and 2 matching images from database on the right (1 blurred and 1 sharp, marked with green boxes).

2.2 Per BL database results (with distractors)

We further present per blur level database retrieval results with the addition of 1M distractors in Fig. 3. This illustration showcases the performance of our model in large-scale retrieval. It should be noted that when both the database blur level and query blur level are 1, the model trained exclusively with sharp images attains a satisfactory score of 89.07, which surpasses the results of state-of-the-art methods (DELG [4]: 86.73, DOLG [47]: 87.01, Token [46]: 88.22), and our model is the sole solution that outperforms it (95.09). This observation suggests that even in large-scale settings and evaluated with mAP@100, training with blurred images does not compromise our model’s retrieval performance for sharp or near-sharp images.

BL Q D	DELG [4] (Range: 51.41; Std: 14.54)							DOLG [47] (Range: 49.99; Std: 14.42)						
	All	1	2	3	4	5	6	All	1	2	3	4	5	6
1	84.52	90.91	89.47	87.59	83.53	76.77	65.05	85.99	90.89	90.46	88.76	85.63	79.45	68.50
2	84.60	88.30	90.08	88.13	84.76	78.04	64.78	85.65	89.11	90.74	88.76	85.97	79.54	67.18
3	84.87	86.94	88.62	88.48	85.87	80.15	67.87	85.90	88.18	89.51	89.01	86.84	81.32	69.79
4	82.93	83.23	85.48	86.17	84.86	80.15	68.49	84.09	85.02	86.69	86.86	85.76	81.09	70.04
5	73.05	70.02	71.70	73.55	74.41	78.98	69.12	74.45	72.25	73.41	74.65	75.46	79.80	70.20
6	46.12	40.95	39.50	42.37	44.48	57.80	67.52	47.06	42.54	40.91	43.16	45.09	58.14	67.98

BL Q D	Token [46] (Range: 49.77; Std: 14.27)							Ours (Range: 46.62 ; Std: 13.51)						
	All	1	2	3	4	5	6	All	1	2	3	4	5	6
1	87.59	92.31	92.26	90.28	87.05	80.95	70.90	93.85	96.31	96.19	95.31	93.73	91.20	83.49
2	87.68	90.76	92.76	90.65	87.79	81.70	70.84	93.66	95.45	96.32	95.15	93.87	91.27	82.90
3	87.78	89.55	91.32	90.75	88.64	83.31	73.44	93.78	95.17	95.65	95.27	94.28	92.03	84.00
4	85.66	86.15	88.10	88.27	87.36	82.68	73.41	92.74	93.50	94.08	94.04	93.57	91.83	84.08
5	75.88	73.72	74.82	75.72	76.70	81.09	73.22	84.05	82.41	82.36	82.89	83.89	90.66	83.93
6	48.91	44.61	42.98	44.75	46.54	59.57	71.09	56.32	52.43	49.70	51.23	52.85	68.08	82.08

Table 1: Retrieval results by query (Q) and database (D) blur level (BL) on our synthetic dataset (without 1M distractors). 'All' denotes the overall performance for queries of all blur levels. The standard deviation and range of mAP values is shown next to each method. The best scores under the same settings are marked in bold.

3 More ablation studies

We conducted extensive experiments on our synthetic dataset with 1M distractors to investigate the impact of different loss components on the retrieval performance of images with different blur levels. The models are categorized into three groups based on the loss function(s) directly applied to the descriptor: those employing solely the contrastive loss \mathcal{L}_{con} , those utilizing only the classification loss \mathcal{L}_{cls} , and those incorporating both. The detailed results are shown in Table 2 and visualizations of results for each database blur level can be found in Fig. 4.

The results of our experiments reveal that within each group of models, utilizing either blur estimation loss \mathcal{L}_{be} or localization loss \mathcal{L}_{loc} alone enhances the model's performance across all blur level settings. Moreover, combining both \mathcal{L}_{be} and \mathcal{L}_{loc} leads to superior overall performance. Additionally, models applying only classification loss directly to the descriptor outperform their counterparts with only contrastive loss directly applied to the descriptor. When compared to models using only \mathcal{L}_{con} or \mathcal{L}_{cls} directly on the descriptor, the combination of both losses applied to the descriptor results in better overall performance. Ultimately, the best overall retrieval performance is achieved when incorporating all four loss components.

4 More qualitative results

In this section, we show more qualitative results for our approach and all compared state-of-the-art retrieval methods in Fig. 5 for synthetic data (with 1M distractors) and in Fig. 6 for real-world data.

These examples highlight the efficacy of our method in object retrieval under the influence of motion blur. State-of-the-art methods tend to retrieve a substantial number of negative images for motion-blurred queries, whereas our approach excels in identifying more positive matches. Furthermore, when comparing the blur levels in the retrieved positive images between our method and others, it can be observed that the images retrieved by our method cover a wider range of blur levels, indicating the superior performance of our approach in learning blur-invariant image representations compared to state-of-the-art retrieval models.

Additionally, the first examples in Fig. 5 and Fig. 6 demonstrate our model’s ability to distinguish intra-class similar objects, while the subsequent examples illustrate its capability for inter-class distinctions. In scenarios where the query object is severely blurred by motion, the retrieval by other methods is notably affected by objects of the same class or, in cases of different classes, by objects with similar textures or shapes. In contrast, our model distinguishes between similar intra-class objects or objects with comparable textures/shapes with higher accuracy, demonstrating its effectiveness in challenging retrieval scenarios.

5 Limitations and future work

Multiple objects in images. Given that our work is the initial exploration of the problem of retrieval in the presence of object motion blur, the focus on single-object scenarios provides a foundational understanding of the challenges associated with this specific task. However, real-world scenarios can involve multiple objects with diverse appearances and motion characteristics. Future work could extend our proposed method to handle cases where multiple objects in an image exhibit different levels of motion blur. This extension would necessitate addressing complexities introduced by the interactions between multiple objects and their varying degrees of blur. Additionally, considering scenarios with multiple objects (possibly overlapping) could open avenues for investigating how the presence of one object’s motion blur affects the retrieval of another object in the scene.

Multiple forms of blur. Our study focuses on retrieval in the presence of object motion blur, which is a common occurrence in various visual scenes. However, other types of blur, such as camera motion-induced blur and out-of-focus blur, are also prevalent phenomena that degrade image quality and likely affect retrieval accuracy. To tackle the broader challenges posed by various types of blur and to enhance the adaptability of retrieval methods across a wider range of scenarios, future research could explore a unified and robust retrieval framework that can effectively handle the integration of multiple forms of blur. Investigating the interplay between different types of blur and their impact on retrieval performance could provide valuable insights into the development of more adaptive and resilient retrieval methodologies.

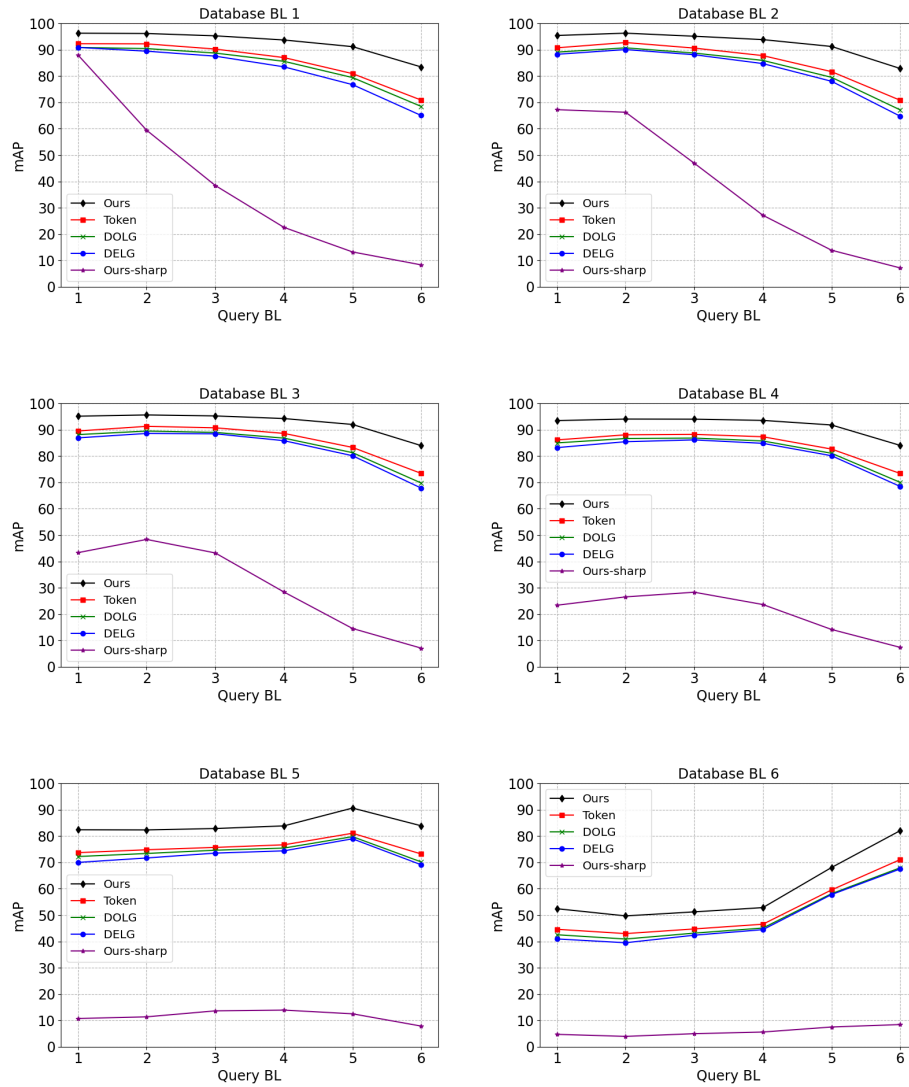


Fig. 2: Retrieval results of different methods by query and database blur level (BL) on our synthetic dataset (without 1M distractors).

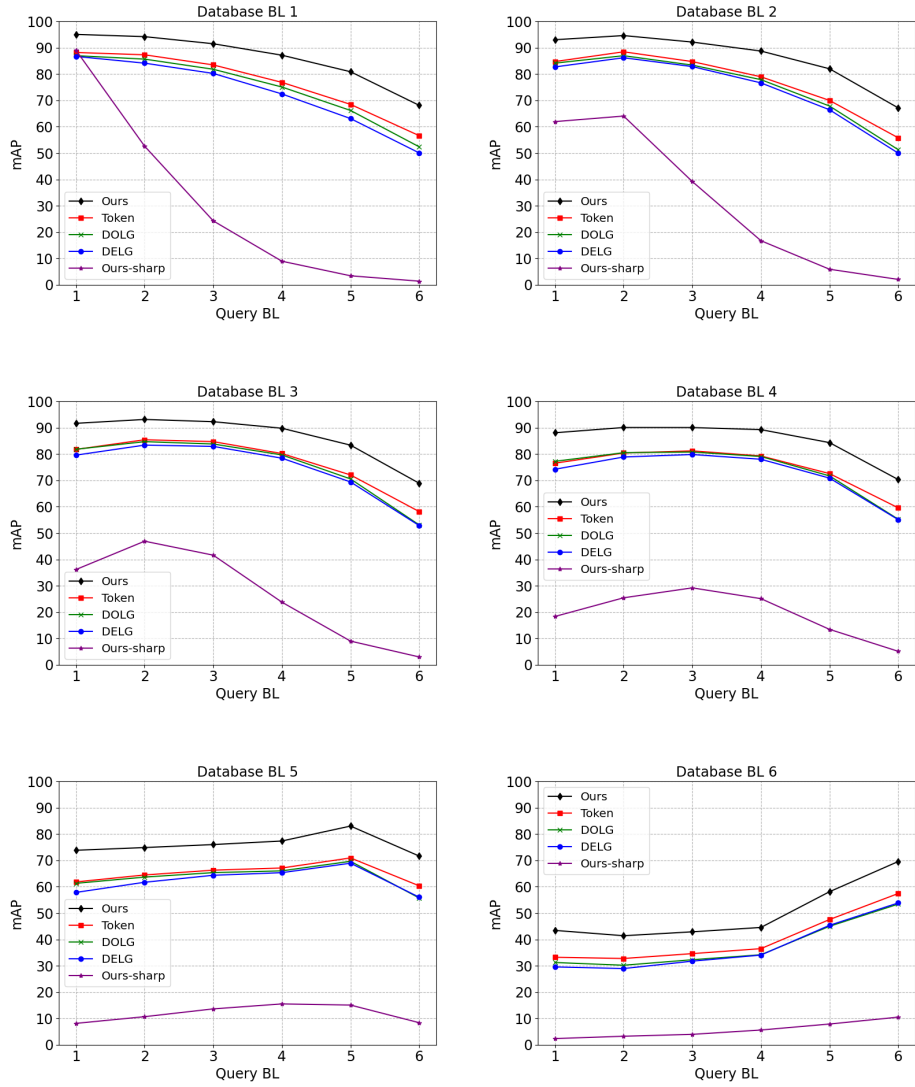


Fig. 3: Retrieval results of different methods by query and database blur level (BL) on our synthetic dataset (with 1M distractors).

BL D/Q	\mathcal{L}_{con}							$\mathcal{L}_{con} + \mathcal{L}_{be}$						
	All	1	2	3	4	5	6	All	1	2	3	4	5	6
1	68.84	80.24	78.56	72.94	64.59	55.39	40.82	71.59	81.70	80.17	75.61	68.55	59.37	44.64
2	70.12	76.63	80.72	75.71	68.28	58.05	40.68	74.01	78.63	83.48	79.41	73.41	63.43	46.83
3	69.67	72.93	77.37	76.21	70.69	60.09	41.70	73.11	75.06	80.33	79.56	74.68	64.54	46.63
4	66.61	66.85	71.90	72.36	69.72	60.96	41.95	70.50	69.37	75.55	75.94	74.08	65.90	47.62
5	54.51	51.82	55.10	56.35	56.73	59.09	42.14	58.89	55.06	59.81	60.79	61.42	63.66	47.42
6	29.05	26.54	25.52	26.86	27.98	35.90	39.70	31.57	28.21	28.10	29.23	30.02	39.16	44.55
BL D/Q	$\mathcal{L}_{con} + \mathcal{L}_{loc}$							$\mathcal{L}_{con} + \mathcal{L}_{be} + \mathcal{L}_{loc}$						
	All	1	2	3	4	5	6	All	1	2	3	4	5	6
1	76.22	83.90	83.05	79.58	74.06	66.53	54.59	77.20	85.30	84.10	80.48	75.09	68.30	53.08
2	76.93	81.59	84.54	81.33	76.06	68.10	54.03	78.93	83.30	86.62	83.16	78.44	71.16	54.21
3	76.16	78.59	82.02	81.22	76.88	69.16	54.40	78.66	81.22	84.55	83.51	79.54	72.28	55.59
4	73.81	73.83	77.56	78.04	76.27	69.96	55.41	76.54	77.00	80.67	80.61	78.77	72.81	56.85
5	63.08	60.48	62.81	64.05	64.84	68.05	54.97	65.93	63.66	66.30	67.14	67.14	70.75	56.55
6	36.76	33.48	32.19	33.74	35.21	45.31	52.01	39.08	35.12	35.28	36.52	37.29	47.65	53.76
BL D/Q	\mathcal{L}_{cls}							$\mathcal{L}_{cls} + \mathcal{L}_{be}$						
	All	1	2	3	4	5	6	All	1	2	3	4	5	6
1	74.00	88.92	86.00	79.61	68.22	55.62	40.36	78.37	92.04	89.31	83.26	73.49	61.37	47.52
2	75.61	85.25	87.75	82.73	73.36	59.14	39.45	81.12	89.09	91.45	87.15	79.51	67.28	50.00
3	75.65	80.81	84.28	83.55	76.88	63.16	41.84	81.33	85.50	88.74	88.02	82.66	70.95	51.92
4	72.48	72.60	77.40	79.04	76.52	66.41	45.51	78.82	78.66	83.25	84.41	82.54	73.87	54.86
5	58.59	53.54	57.33	60.53	62.00	65.47	49.45	65.89	60.81	64.65	67.29	69.11	73.28	57.67
6	30.00	24.94	23.56	26.59	29.15	40.88	49.35	36.83	31.73	30.71	33.38	35.56	47.76	56.63
BL D/Q	$\mathcal{L}_{cls} + \mathcal{L}_{loc}$							$\mathcal{L}_{cls} + \mathcal{L}_{be} + \mathcal{L}_{loc}$						
	All	1	2	3	4	5	6	All	1	2	3	4	5	6
1	83.27	90.92	89.68	86.60	81.12	73.93	62.18	86.29	92.72	91.90	89.14	84.65	78.21	67.90
2	84.22	88.96	91.14	88.25	83.83	75.99	61.38	86.97	90.79	93.02	90.55	86.49	80.00	67.66
3	84.23	86.89	89.20	88.69	85.43	77.95	63.02	86.82	88.83	91.27	90.74	87.61	81.46	69.12
4	82.53	82.75	85.61	86.28	85.12	79.18	65.19	85.22	85.12	88.19	88.59	87.23	82.20	70.76
5	71.03	67.31	69.44	71.63	72.86	77.83	66.50	74.47	71.02	73.24	74.65	75.88	80.79	71.23
6	41.87	36.45	35.29	38.18	40.20	53.16	64.45	45.96	40.82	39.76	42.05	43.68	57.04	69.29
BL D/Q	$\mathcal{L}_{con} + \mathcal{L}_{cls}$							$\mathcal{L}_{con} + \mathcal{L}_{cls} + \mathcal{L}_{be}$						
	All	1	2	3	4	5	6	All	1	2	3	4	5	6
1	80.67	91.14	89.81	85.39	77.65	67.19	51.88	82.75	92.28	91.15	87.19	80.07	71.03	54.90
2	81.74	88.18	90.82	87.53	80.91	70.34	51.92	83.83	89.37	92.35	89.03	83.39	73.94	55.40
3	81.54	84.96	88.48	87.63	82.96	72.66	53.74	83.72	86.75	90.16	89.32	85.17	75.85	57.48
4	79.34	79.78	84.01	84.46	82.48	74.42	55.72	81.65	81.70	86.18	86.47	84.80	77.28	59.19
5	66.77	63.31	66.52	68.17	68.89	72.88	56.95	69.68	65.72	69.22	71.13	72.12	75.96	60.41
6	37.87	34.05	33.07	34.68	35.91	47.25	55.04	39.22	34.70	33.70	35.84	37.53	49.43	58.18
BL D/Q	$\mathcal{L}_{con} + \mathcal{L}_{cls} + \mathcal{L}_{loc}$							$\mathcal{L}_{con} + \mathcal{L}_{cls} + \mathcal{L}_{be} + \mathcal{L}_{loc}$						
	All	1	2	3	4	5	6	All	1	2	3	4	5	6
1	86.28	93.44	92.71	89.56	85.10	77.67	62.86	88.57	95.09	94.24	91.54	87.19	80.91	68.15
2	86.77	91.42	93.52	90.56	86.99	79.13	62.62	88.75	93.07	94.65	92.18	88.77	82.03	67.18
3	86.84	89.86	91.91	90.81	88.20	80.81	64.80	88.76	91.70	93.18	92.32	89.83	83.41	68.94
4	85.28	86.03	88.71	88.63	87.72	82.04	66.90	87.16	88.12	90.11	90.09	89.31	84.37	70.35
5	74.31	71.45	73.26	74.69	75.89	80.66	68.19	76.28	73.87	74.90	76.04	77.39	83.06	71.67
6	45.21	40.98	39.22	41.32	43.03	55.74	66.50	47.31	43.43	41.41	42.89	44.55	58.13	69.59

Table 2: Ablation study on the impact of different loss components on the retrieval performance of images with different blur levels (BLs), conducted on our synthetic dataset (with 1M distractors). The best scores under the same BL settings are marked in blue (comparing models w/o \mathcal{L}_{cls}), green (comparing models w/o \mathcal{L}_{con}), red (comparing models with $\mathcal{L}_{cls} + \mathcal{L}_{con}$), or bold (comparing all models).

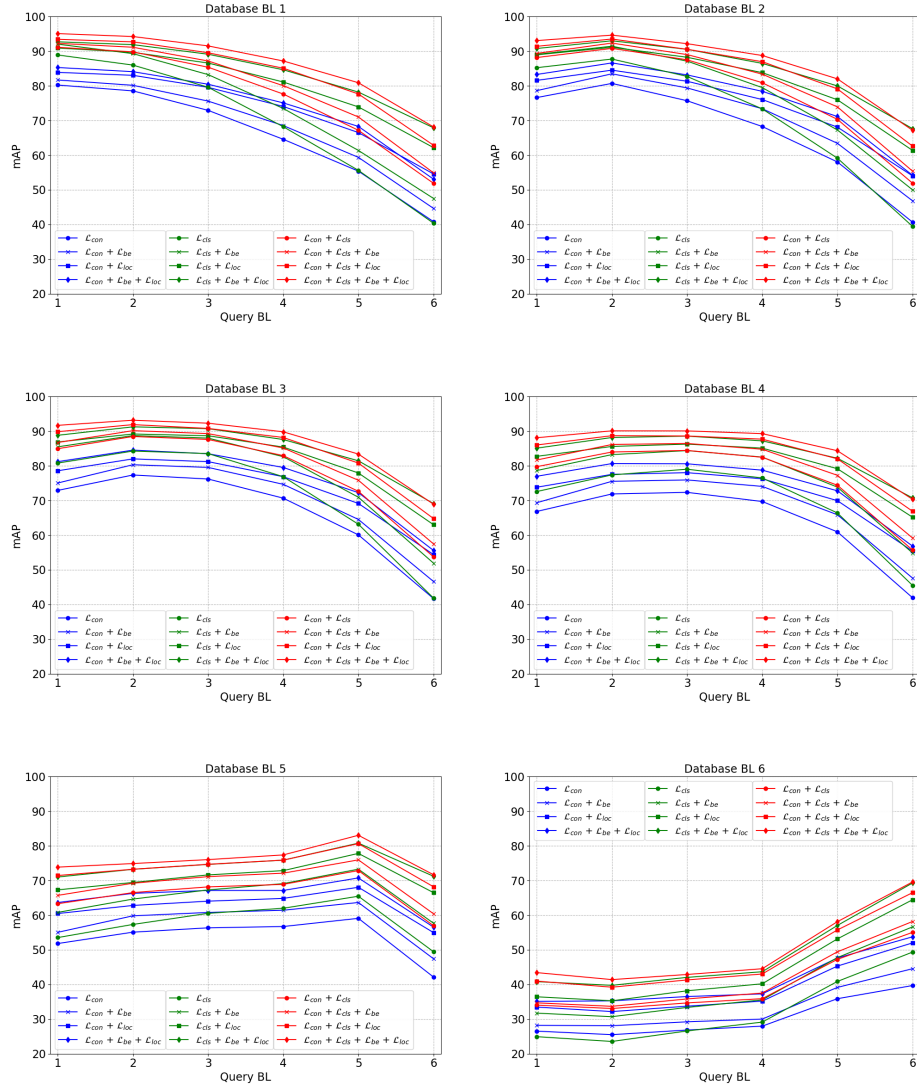


Fig. 4: Ablation study investigating the influence of distinct loss components on the retrieval performance of images with different blur levels (BLs), carried out on our synthetic dataset (with 1M distractors). The results for each database BL are categorized into three groups: models without \mathcal{L}_{cls} , marked in blue, models without \mathcal{L}_{con} , marked in green, and models with both \mathcal{L}_{cls} and \mathcal{L}_{con} , marked in red.



Fig. 5: Comparison of retrieval results between our approach and state-of-the-art retrieval methods on our synthetic dataset (with 1M distractors). The retrieved images are sorted from left to right, top to bottom, with the ranking from the 1st to the 20th. The blur level of each image is shown in bottom left corner. Correct results are indicated with green boxes, while incorrect ones are marked with red boxes.

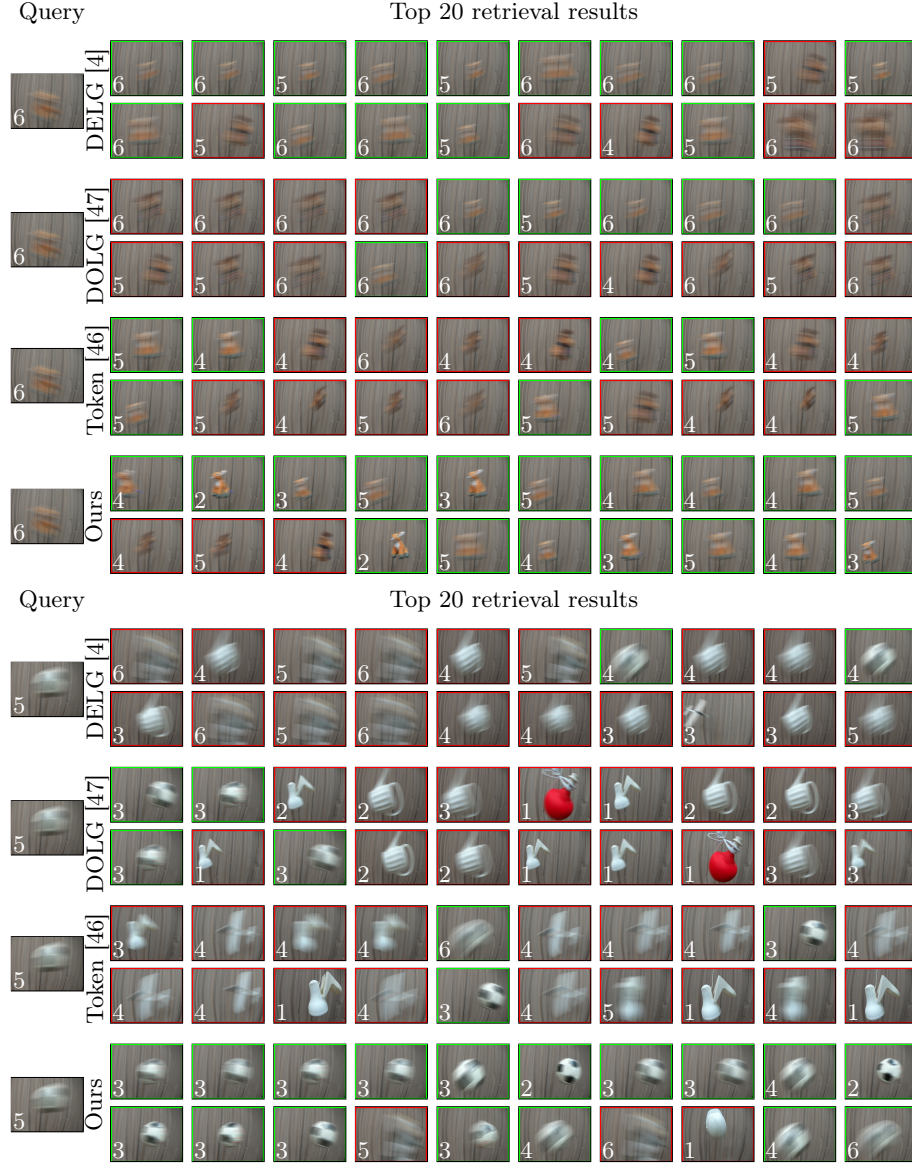


Fig. 6: Comparison of retrieval results between our approach and state-of-the-art retrieval methods on our real-world dataset. The retrieved images are sorted from left to right, top to bottom, with the ranking from the 1st to the 20th. The blur level of each image is shown in bottom left corner. Correct results are indicated with green boxes, while incorrect ones are marked with red boxes.

References

1. Babenko, A., Lempitsky, V.: Aggregating local deep features for image retrieval. In: ICCV. pp. 1269–1277 (2015)
2. Babenko, A., Slesarev, A., Chigorin, A., Lempitsky, V.: Neural codes for image retrieval. In: ECCV. pp. 584–599. Springer (2014)
3. Bay, H., Ess, A., Tuytelaars, T., Van Gool, L.: Speeded-up robust features (surf). *Computer Vision and Image Understanding* **110**(3), 346–359 (2008)
4. Cao, B., Araujo, A., Sim, J.: Unifying deep local and global features for image search. In: Vedaldi, A., Bischof, H., Brox, T., Frahm, J.M. (eds.) ECCV. pp. 726–743. Springer International Publishing, Cham (2020)
5. Chang, A.X., Funkhouser, T., Guibas, L., Hanrahan, P., Huang, Q., Li, Z., Savarese, S., Savva, M., Song, S., Su, H., Xiao, J., Yi, L., Yu, F.: ShapeNet: An Information-Rich 3D Model Repository. Tech. Rep. arXiv:1512.03012 [cs.GR], Stanford University — Princeton University — Toyota Technological Institute at Chicago (2015)
6. Chopra, S., Hadsell, R., LeCun, Y.: Learning a similarity metric discriminatively, with application to face verification. In: CVPR. vol. 1, pp. 539–546. IEEE (2005)
7. Community, B.O.: Blender - a 3D modelling and rendering package. Blender Foundation, Stichting Blender Foundation, Amsterdam (2018), <http://www.blender.org>
8. Deng, J., Dong, W., Socher, R., Li, L.J., Li, K., Fei-Fei, L.: ImageNet: A Large-Scale Hierarchical Image Database. In: CVPR (2009)
9. Deng, J., Guo, J., Xue, N., Zafeiriou, S.: Arcface: Additive angular margin loss for deep face recognition. In: 2019 IEEE/CVF Conference on Computer Vision and Pattern Recognition (CVPR). pp. 4685–4694 (2019). <https://doi.org/10.1109/CVPR.2019.00482>
10. Gong, D., Yang, J., Liu, L., Zhang, Y., Reid, I., Shen, C., Van Den Hengel, A., Shi, Q.: From motion blur to motion flow: A deep learning solution for removing heterogeneous motion blur. In: CVPR. pp. 3806–3815 (2017). <https://doi.org/10.1109/CVPR.2017.405>
11. Gordo, A., Almazan, J., Revaud, J., Larlus, D.: Deep image retrieval: Learning global representations for image search (2016)
12. He, K., Zhang, X., Ren, S., Sun, J.: Deep residual learning for image recognition. In: CVPR. pp. 770–778 (2016)
13. Hendrycks, D., Dietterich, T.: Benchmarking neural network robustness to common corruptions and perturbations. *Proceedings of the International Conference on Learning Representations* (2019)
14. Jaesung, R., Haeyun, L., Jucheol, W., Sunghyun, C.: Real-world blur dataset for learning and benchmarking deblurring algorithms. In: ECCV (2020)
15. Jégou, H., Perronnin, F., Douze, M., Sánchez, J., Pérez, P., Schmid, C.: Aggregating local image descriptors into compact codes. *IEEE TPAMI* **34**(9), 1704–1716 (2011)
16. Kalantidis, Y., Mellina, C., Osindero, S.: Cross-dimensional weighting for aggregated deep convolutional features. pp. 685–701. Springer (2016)
17. Kingma, D.P., Ba, J.: Adam: A method for stochastic optimization. In: Bengio, Y., LeCun, Y. (eds.) ICLR (2015), <http://arxiv.org/abs/1412.6980>
18. Kotera, J., Rozumnyi, D., Šroubek, F., Matas, J.: Intra-frame object tracking by deblatting (Oct 2019)

19. Kupyn, O., Budzan, V., Mykhailych, M., Mishkin, D., Matas, J.: Deblurgan: Blind motion deblurring using conditional adversarial networks. In: CVPR (June 2018)
20. Lee, S., Seong, H., Lee, S., Kim, E.: Correlation verification for image retrieval. In: CVPR. pp. 5374–5384 (2022)
21. Lowe, D.G.: Distinctive image features from scale-invariant keypoints. *IJCV* **60**, 91–110 (2004)
22. Michaelis, C., Mitzkus, B., Geirhos, R., Rusak, E., Bringmann, O., Ecker, A.S., Bethge, M., Brendel, W.: Benchmarking robustness in object detection: Autonomous driving when winter is coming. arXiv preprint arXiv:1907.07484 (2019)
23. Nah, S., Kim, T.H., Lee, K.M.: Deep multi-scale convolutional neural network for dynamic scene deblurring. In: CVPR (July 2017)
24. Noh, H., Araujo, A., Sim, J., Weyand, T., Han, B.: Large-scale image retrieval with attentive deep local features. In: ICCV. pp. 3456–3465 (2017)
25. Paszke, A., Gross, S., Massa, F., Lerer, A., Bradbury, J., Chanan, G., Killeen, T., Lin, Z., Gimelshein, N., Antiga, L., Desmaison, A., Kopf, A., Yang, E., DeVito, Z., Raison, M., Tejani, A., Chilamkurthy, S., Steiner, B., Fang, L., Bai, J., Chintala, S.: Pytorch: An imperative style, high-performance deep learning library. In: Wallach, H., Larochelle, H., Beygelzimer, A., Alché-Buc, F., Fox, E., Garnett, R. (eds.) NeurIPS, pp. 8024–8035. Curran Associates, Inc. (2019), <http://papers.neurips.cc/paper/9015-pytorch-an-imperative-style-high-performance-deep-learning-library.pdf>
26. Perronnin, F., Liu, Y., Sánchez, J., Poirier, H.: Large-scale image retrieval with compressed fisher vectors. In: CVPR. pp. 3384–3391. IEEE (2010)
27. Radenović, F., Iscen, A., Tolias, G., Avrithis, Y., Chum, O.: Revisiting oxford and paris: Large-scale image retrieval benchmarking. In: CVPR. pp. 5706–5715 (2018)
28. Radenović, F., Tolias, G., Chum, O.: Fine-tuning cnn image retrieval with no human annotation. arXiv preprint arXiv:1711.02512 (2017)
29. Radenović, F., Tolias, G., Chum, O.: Fine-tuning cnn image retrieval with no human annotation. *IEEE TPAMI* **41**(7), 1655–1668 (2019). <https://doi.org/10.1109/TPAMI.2018.2846566>
30. Rozumnyi, D., Kotera, J., Šroubek, F., Matas, J.: Non-causal tracking by deblatting. pp. 122–135. Springer International Publishing, Cham (2019)
31. Rozumnyi, D., Kotera, J., Šroubek, F., Novotný, L., Matas, J.: The world of fast moving objects. In: CVPR. pp. 4838–4846 (July 2017). <https://doi.org/10.1109/CVPR.2017.514>
32. Rozumnyi, D., Kotera, J., Šroubek, F., Matas, J.: Sub-frame appearance and 6d pose estimation of fast moving objects. In: CVPR. pp. 6777–6785 (2020)
33. Rozumnyi, D., Oswald, M.R., Ferrari, V., Matas, J., Pollefeys, M.: Defmo: Deblurring and shape recovery of fast moving objects. In: CVPR. Nashville, Tennessee, USA (Jun 2021)
34. Rozumnyi, D., Oswald, M.R., Ferrari, V., Pollefeys, M.: Shape from blur: Recovering textured 3d shape and motion of fast moving objects. In: NeurIPS (2021)
35. Rozumnyi, D., Oswald, M.R., Ferrari, V., Pollefeys, M.: Motion-from-blur: 3d shape and motion estimation of motion-blurred objects in videos. In: CVPR (Jun 2022)
36. Sayed, M., Brostow, G.: Improved handling of motion blur in online object detection. In: CVPR. pp. 1706–1716 (June 2021)
37. Sivic, Zisserman: Video google: A text retrieval approach to object matching in videos. In: ICCV. pp. 1470–1477. IEEE (2003)
38. Skorokhodov, I., Sotnikov, G., Elhoseiny, M.: Aligning latent and image spaces to connect the unconnectable. In: ICCV. pp. 14144–14153 (2021)

39. Tolias, G., Avrithis, Y., Jégou, H.: Image search with selective match kernels: aggregation across single and multiple images. *IJCV* **116**, 247–261 (2016)
40. Tolias, G., Jenicek, T., Chum, O.: Learning and aggregating deep local descriptors for instance-level recognition. In: *ECCV*. pp. 460–477. Springer (2020)
41. Tolias, G., Jenicek, T., Chum, O.: Learning and aggregating deep local descriptors for instance-level recognition. In: *ECCV*. pp. 460–477. Springer (2020)
42. Tolias, G., Sicre, R., Jégou, H.: Particular object retrieval with integral max-pooling of cnn activations. *ICLR* (2016)
43. Vasiljevic, I., Chakrabarti, A., Shakhnarovich, G.: Examining the impact of blur on recognition by convolutional networks. arXiv preprint arXiv:1611.05760 (2016)
44. Wang, Y., Lu, Y., Gao, Y., Wang, L., Zhong, Z., Zheng, Y., Yamashita, A.: Efficient video deblurring guided by motion magnitude. In: *ECCV*. pp. 413–429. Springer (2022)
45. Weyand, T., Araujo, A., Cao, B., Sim, J.: Google landmarks dataset v2—a large-scale benchmark for instance-level recognition and retrieval. In: *CVPR*. pp. 2574–2583 (2020)
46. Wu, H., Wang, M., Zhou, W.T., Hu, Y., Li, H.: Learning token-based representation for image retrieval. In: *AAAI Conference on Artificial Intelligence* (2021), <https://api.semanticscholar.org/CorpusID:245124518>
47. Yang, M., He, D., Fan, M., Shi, B., Xue, X., Li, F., Ding, E., Huang, J.: Dolg: Single-stage image retrieval with deep orthogonal fusion of local and global features. In: *ICCV*. pp. 11752–11761. IEEE Computer Society, Los Alamitos, CA, USA (oct 2021). <https://doi.org/10.1109/ICCV48922.2021.01156>, <https://doi.ieeecomputersociety.org/10.1109/ICCV48922.2021.01156>
48. Yokoo, S., Ozaki, K., Simo-Serra, E., Iizuka, S.: Two-stage discriminative re-ranking for large-scale landmark retrieval. In: *CVPRW*. IEEE (2020)
49. Zhang, H., Xie, H., Yao, H.: Spatio-temporal deformable attention network for video deblurring. In: *ECCV*. pp. 581–596. Springer (2022)
50. Zhou, S., Zhang, J., Pan, J., Xie, H., Zuo, W., Ren, J.: Spatio-temporal filter adaptive network for video deblurring. In: *ICCV* (2019)